Organic Electronics 11 (2010) 1318–1322

Contents lists available at ScienceDirect

Organic Electronics

journal homepage: www.elsevier.com/locate/orgel

Letter

High spectrum selectivity organic/inorganic hybrid visible-blind ultraviolet photodetector based on ZnO nanorods

Lidan Wang [a,b], Dongxu Zhao [a,*], Zisheng Su [a], Fang Fang [a], Binghui Li [a], Zhenzhong Zhang [a], Dezhen Shen [a], Xiaohua Wang [c]

[a] Key Laboratory of Excited State Processes, Changchun Institute of Optics, Fine Mechanics and Physics, Chinese Academy of Sciences, Changchun 130033, People's Republic of China
[b] Graduate School of Chinese Academy of Sciences, Beijing 100039, People's Republic of China
[c] School of Science, Changchun University of Science and Technology, 7089 Wei-Xing Road, Changchun 130022, People's Republic of China

ARTICLE INFO

Article history:
Received 23 February 2010
Received in revised form 9 April 2010
Accepted 11 April 2010
Available online 18 April 2010

Keywords:
Zinc oxide
Hybrid
Photodetector
Nanorods

ABSTRACT

The authors demonstrated high spectrum selectivity hybrid ultraviolet (UV) photodetector (PD) by using electrodeposited ZnO nanorods and poly-*N*-vinylcarbazole as the electron acceptor and donor, respectively. The photoresponse of the PD showed a narrow band centered at 364 nm with a full width at half maximum of only 26 nm, which was attributed to the absorption of ZnO nanorods. An ultraviolet–visible rejection ratio (R364/R400 nm) of three orders of magnitude was also obtained at −5 V bias. Those results provided a simple route to fabricate low-cost high spectrum selectivity hybrid visible-blind UV-PDs.

1. Introduction

Zinc oxide (ZnO) has been regarded as an excellent semiconductor material for the ultraviolet (UV) detection due to its wide band gap of 3.37 eV as well as the high chemical and thermal stability [1–3]. Compared with ZnO bulk materials, one dimensional (1D) nanostructures may offer additional advantages for optoelectronic devices due to the increased junction area, the enhanced polarization dependence, and the improved carrier confinement in one dimension. Different devices based on ZnO 1D nanostructures were successfully realized, such as UV detectors, light emitting diodes [4], solar cells [5,6], gas sensors [7] and transistors [8,9]. UV detectors based on an individual ZnO 1D nanostructure presented high internal photoconductive gain and high sensitivity. And for the ZnO 1D nanostructure arrays, a heterojunction UV detector with using a *p*-type polymer as the hole collection and transport layer was constructed. This polymer-inorganic hybrid photodetectors (PDs) combined the solution processability of polymers with the high electron mobility of inorganic semiconductors [10]. For the hybrid ZnO based PDs, the optical properties of polymers played an important role for the device performance. For example, in a previous report [11] the photoresponse extended to the visible region under a high operation voltage because of the absorption of the polymer. Concerning this point, polymers with the absorption band in the short-wavelength region should be used. And we noticed almost for all the ZnO based UV detectors, the photoresponse covered a broad spectral region [11,12]. However, for practical applications a high spectrum selectivity is particularly desired. Considering the above two points, we constructed an ITO/ZnO/poly-*N*-vinylcarbazole (PVK) hybrid device with a high photoresponse spectrum selectivity, in which the ITO glass and PVK acted as filters to make a cut-off in the short-wavelength region (shorter than 350 nm).

* Corresponding author. Tel.: +86 431 86176322; fax: +86 431 84627031.
E-mail address: dxzhao2000@yahoo.com.cn (D. Zhao).

1566-1199/$ - see front matter © 2010 Elsevier B.V. All rights reserved.
doi:10.1016/j.orgel.2010.04.010

2. Experimental

Among the various techniques to grow 1D ZnO nanostructures, the cost-effective electrodeposition method was used in this work for the preparation of large area of nanorods because of the low-temperature processing, arbitrary substrate shapes, and precise control of the size of nanorods. ZnO nanorods were electrodeposited in 0.005 M $Zn(NO_3)_2$ and 0.005 M hexamethylenetramine aqueous solutions. Devices were fabricated on cleaned indium tin oxide (ITO) coated glass substrates with a sheet resistance of 25 Ω/□. All depositions were carried out in a configured glass cell at 90 °C, in which an ITO substrate, a platinum plate, and a Ag/AgCl electrode in saturated KCl served as the working electrode, the counter electrode and the reference electrode, respectively. All electrodepositions were done at a potential of −0.9 V vs. the reference electrode. The durations of the deposition were 20 min. PVK (10 mg/ml) was spin-coated onto ZnO nanorods at 800 r/min. Then films were baked in a vacuum oven for 30 min at 100 °C. A thin layer of poly(3,4-ethylenedioxythiophene)-poly(styrenesulfonate) (PEDOT:PSS) was spin-coated on the PVK film at 2000 r/min. After this step the films were baked in a vacuum oven for 1 h at 120 °C. Finally, Au was evaporated onto the device as the top electrode. The field emission scanning electron microscopy (FESEM) measurements were performed on the Hitachi FESEM S-4800. The optical transmission spectra and the absorption spectra were recorded using a Shimadzu UV-3101PC spectrophotometer. The photoluminescence (PL) measurement was carried out in a JY-630 micro-Raman spectrometer employing the 325 nm line of a He–Cd laser as the excitation source. The photoresponse of the ZnO nanorods/PVK hybrid photodetector was studied using a 150 W Xe lamp, a monochromator, a chopper (EG&G 192), and a lock-in amplifier (EG&G 124A). Current–voltage (*I*–*V*) characteristics of the devices were measured using a Keithley 2400 source meter connected with a GPIB controller to a computer under dark or illumination at 365 nm. PL decay time was measured using an Edinburgh FL 920 Spectrometer, in which the exciting wavelength was 325 nm by using a hydrogen lamp and the PL emission wavelength was probed at 380 nm. All the measurements were carried out at room temperature under ambient conditions.

3. Results and discussion

Fig. 1(a) shows the typical FESEM image of ZnO nanorods almost aligned vertically on the ITO substrate. The diameter and the length of the nanorods are in the ranges of 20–40 and 800–1000 nm, respectively. Fig. 1(b) shows the PL spectra of the ZnO nanorods excited by the 325 nm line of a He–Cd laser. In the PL spectrum, a strong and sharp UV near-band-emission is observed with a peak centered at 378 nm, which is explained by the recombination of free excitons [13,14]. Meanwhile, a weak deep level green emission is found. The origin of the deep level emission in ZnO is not yet clearly understood but is generally

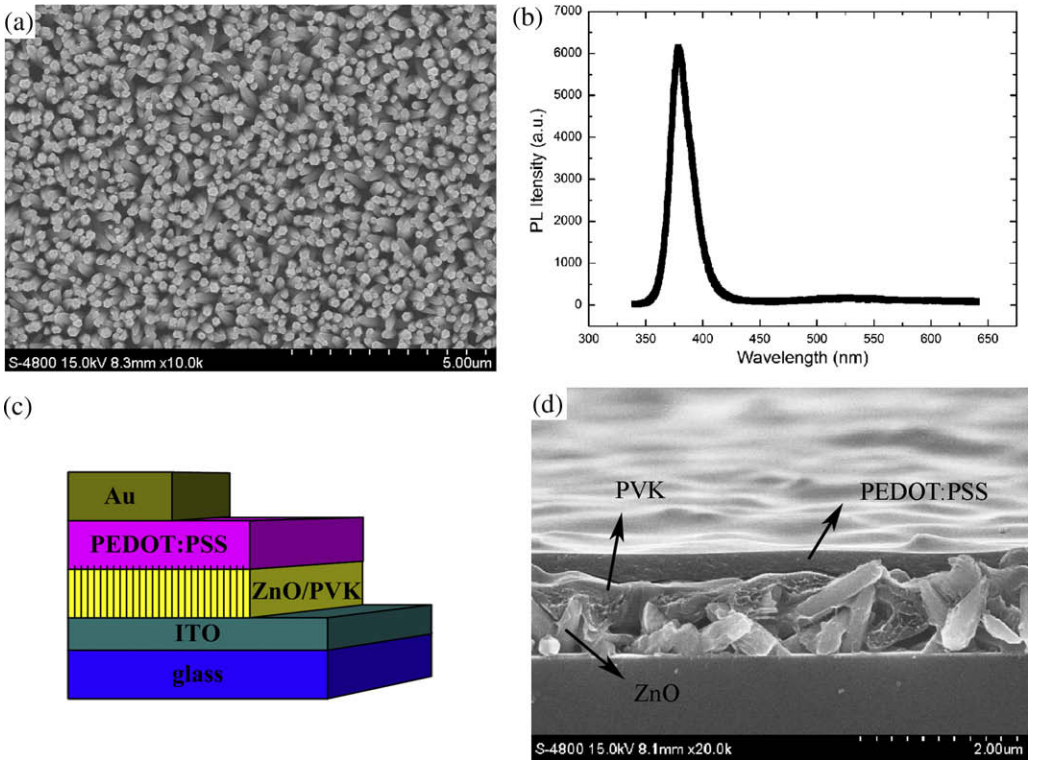

Fig. 1. (a) The FESEM image of ZnO nanorods. The scale bar is 5 μm. (b) The PL spectra of the ZnO nanorods. (c) The schematic diagram of the ZnO/PVK hybrid device. (d) The cross-section field emission SEM images of ZnO nanorods after covered with PVK and PEDOT:PSS by spin-coating. The scale bar is 2 μm.

attributed to structural defects, single ionized vacancies, and impurities [15]. The excellent optical properties of ZnO nanorods, deduced from the strong and sharp excitonic emission and the low deep level emission, indicate that the ZnO nanorods are of high optical quality, making them more suitable for fabricating UV-PDs. Fig. 1(c) shows the schematic diagram of the ZnO/PVK hybrid device. From the cross-section FESEM image shown in Fig. 1(d), different layers could be observed clearly. ZnO nanorods are completely covered with PVK and PEDOT:PSS. And the Au electrode does not directly connected with nanorods, which ensures a junction could be formed between ZnO nanorods and PVK.

The *I–V* characteristics of the ZnO/PVK heterojunction device measured in the dark is shown in Fig. 2. The current density of the device increases gradually with the bias voltage, and a typical *p–n* junction behavior with the clearly rectifying *I–V* characteristics was found, indicating the formation of a *p–n* junction interfaces between the PVK and ZnO nanorods. The *I–V* characteristics of the PD under illumination of a 1.2 mW/cm^2 365 nm UV lamp was also shown in Fig. 2. A maximum current density of 132 μA/cm^2 is obtained at −5 V bias, corresponding to a response of 110 mA/W.

Fig. 3(a) shows the absorption spectra of ZnO nanorods and PVK and the transmission spectrum of the ITO glass. It could be observed that the transmission of ITO glass is as high as 80%, when the wavelength is longer than 350 nm. And there is a sharp absorption edge for the wavelength shorter than 350 nm. For PVK a strong absorption band presents between 320 and 350 nm, and there is no absorption for the light wavelength longer than 360 nm. The absorption spectrum of ZnO nanorods shows a typical semiconductor property. A sharp absorption edge located at 380 nm could be clearly detected. Fig. 3(b) shows the photoresponse spectra of the device illuminated from both the ITO glass and Au electrode sides. As shown in the figure, the photoresponse of the PD illuminated from ITO glass presents a peak at 364 nm with a weak shoulder at around 335 nm. It is interesting to found that the photoresponse is a narrow band with a full width at half maximum (FWHM) of only 26 nm, indicating a high spectrum selectivity property of the PD. At the same time a very sharp cutting-off at about 400 nm is observed in the photoresponse spectrum. The ultraviolet–visible rejection ratio (R364/R400 nm) for the devices is as high as 10^3. While the PD illuminated from Au electrode the photoresponse shows the same shape (shown in the insert of Fig. 3), but a little broader in the short-wavelength region than the one illuminated from ITO glass side. And the intensity of the photoresponse peak is lowered one order of magnitude because of the high reflection for the Au electrode.

Due to the absorption peak of PVK is predominantly located in the range of 320–350 nm, the photoresponse of the PD at 335 nm could be deduced originated from PVK. Based on the absorption and transmission spectra shown in the Fig. 3(a), there are no absorptions for PVK and ITO for the light wavelength longer than 360 nm. Only ZnO has the absorption edge of 380 nm, which is in agreement with other reports [11,16]. Thus, the photoresponse peak located at 364 nm could be attributed to the absorption of the ZnO nanorods. When illuminated from the ITO side the light would meet ZnO at first and most UV light could be absorbed by ZnO nanorods, which induces the photoresponse for the wavelength smaller than 400 nm. A part of UV light with the wavelength shorter than 360 nm could reach the PVK layer to form another photoresponse peak

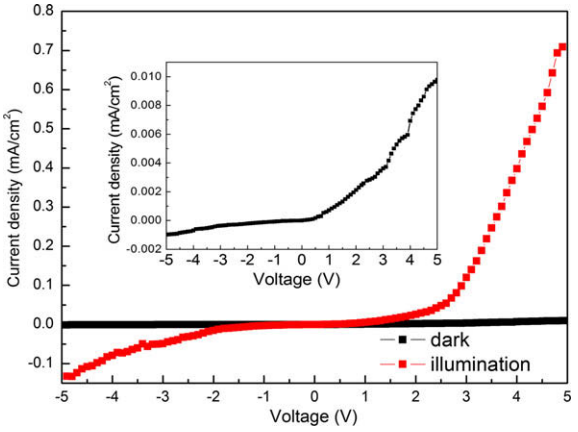

Fig. 2. The current–voltage characteristics of the ZnO/PVK heterojunction diode measured in the dark and under illumination at 365 nm, respectively. The inset shows the current–voltage characteristics of the ZnO/PVK heterojunction diode individually measured in the dark.

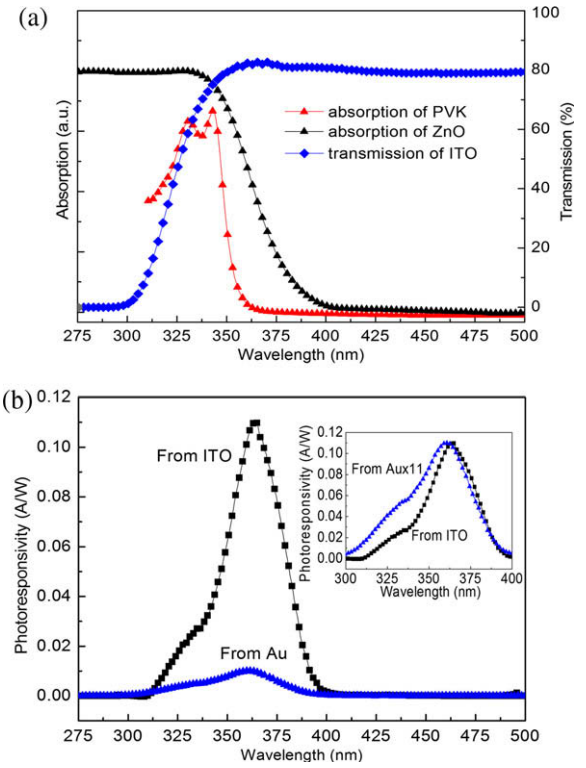

Fig. 3. (a) The absorption spectra of ZnO nanorods and PVK and the transmission spectrum of the ITO glass. (b) The photoresponse spectra of the device illuminated from both the ITO glass and Au electrode. The inset shows the shape comparison of the photoresponse spectra of the device illuminated from the ITO glass and Au electrode.

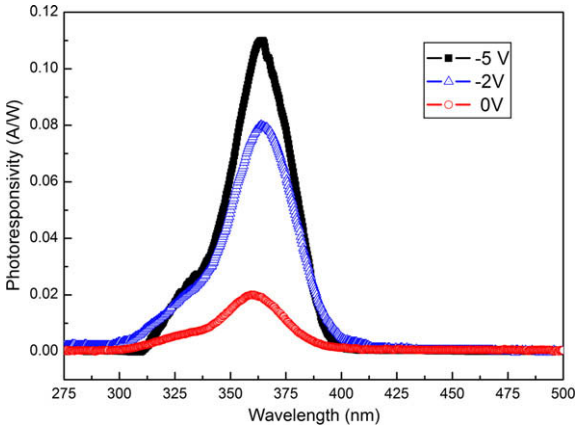

Fig. 4. The photoresponse spectra of the device illuminated from the ITO glass at different biases.

at 335 nm. But when illustrated from the Au side, the light would meet the PVK layer at first, which induced the intensity ratio of the photoresponse peaks located at 335 and 364 nm became increased a little. And in both cases, the ITO glass and the PVK layer serve as filters when the wavelength of the incident light shorter than 350 nm, which induced the weak photoresponse for the device in the short-wavelength region. Fig. 4 shows the photoresponse spectra of the device at different biases, in which the position of the photoresponse band keeps almost unchanged. This result conforms the active region of PDs is ZnO nanorods.

To further understand the charge transfer processes in the ZnO/PVK hybrid system, the PL spectra of the ZnO nanorods, PVK pristine film, and the ZnO nanorods/PVK hybrid film and the PL decay spectra of the PVK pristine film, and the ZnO nanorods/PVK hybrid film were investigated, as shown in Fig. 5. The PL spectra of ZnO nanorods and PVK pristine film showed emission peaks located at 380 and 410 nm, respectively. The PL intensity of the ZnO nanorods/PVK hybrid film is dramatically reduced compared with both the ZnO nanorods and the PVK pristine film, which indicates an efficient charge transfer process from ZnO to PVK and PVK to ZnO. (In order to make the PL spectra comparable, all the condition, such as the sample position, the wide of slid, the power of incident light, et al., were kept the same.)

The transient PL decay measurements were carried out for the PVK pristine film, and the ZnO nanorods/PVK hybrid film. The decay curves were shown in Fig. 5(b). The exciting light was illuminated from the PVK side for the ZnO/PVK hybrid sample. Although from the PL spectra shown in Fig. 5(a), both ZnO and PVK have the PL emission at 380 nm, the signals of the PL decay time measurement were mainly from the PVK layer. By fitting these curves, decay times can be obtained, PVK shows an exponential decay with a decay time of 27.95 ± 0.92 ns. In the ZnO nanorods/PVK hybrid film, a shorter decay time of 21.74 ± 0.76 ns ascribe to PVK were obtained. The shortened lifetimes indicate a new deactivation pathway for the excited state. The ZnO emission decay reflects the charge recombination via radiative and nonradiative processes. With constructing the ZnO/PVK hybrid system an additional pathway is introduced through the electronic coupling in the interface of ZnO and PVK.

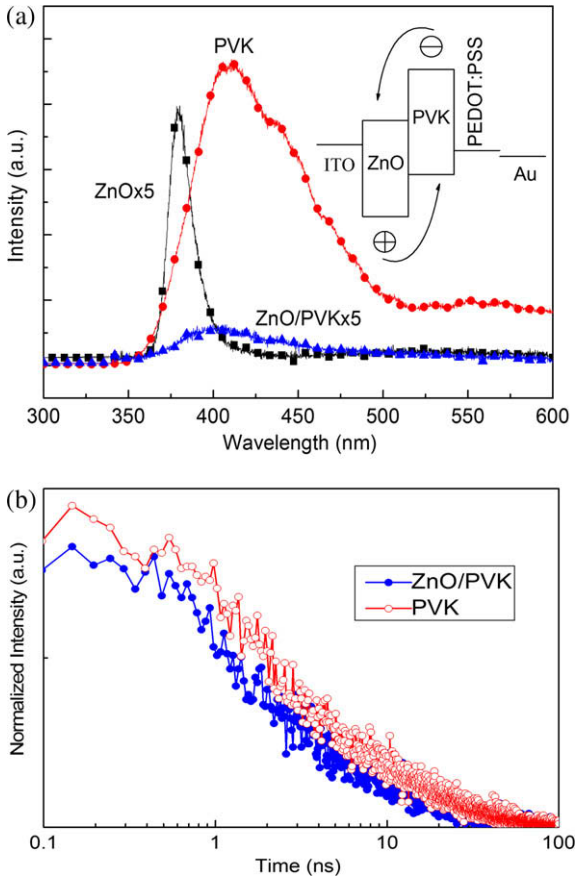

Fig. 5. (a) The PL spectra of ZnO nanorods, PVK layer and ZnO/PVK. The inset shows the corresponding energy levels for the materials used in the hybrid device. (b) The decay curve of PVK and ZnO/PVK hybrid film. The exciting wavelength was chosen at 325 nm, and the PL emission wavelength was probed at 380 nm.

The inset of Fig. 5(a) shows the charge carriers generation processes in the UV-PDs. Under the illumination of UV lamp, photogenerated electron–hole pairs are produced in both ZnO nanorods and PVK. The holes in ZnO nanorods will migrate from the valance band to the highest occupied molecular orbital (HOMO) of PVK due to the higher HOMO of PVK (5.8 eV) than the valance band of ZnO (7.2 eV), while the electrons in PVK will migrate from the LUMO to the conduction band of ZnO due to the lower conduction band of ZnO (4.0 eV) than the LUMO of PVK (2.3 eV) [17]. Then the holes and electrons in the PVK HOMO and ZnO conduction band will transport to the Au and ITO electrodes, respectively. The energy level matching between ZnO and PVK facilitates the fast interfacial charge transfer and increases the separation efficiency of electron–hole pairs and the carrier generation efficiency. Such an interfacial charge transfer between ZnO nanorods and PVK reduces the probability of the recombination of electron and hole. Due to the above charge transfer and separation processes the PL intensity is decreased and the photoresponse is promoted.

4. Conclusions

In summary, high spectrum selectivity visible-blind UV-PD based on ZnO nanorods was demonstrated. The photo-response showed a narrow band centered at 364 nm with a FWHM of only 26 nm. This finding has potential values for further study of high spectrum selectivity and low-cost PD since the complete processes are compatible for large area and flexible substrate fabrications.

Acknowledgments

This work is supported by the Key Project of National Natural Science Foundation of China under Grant No. 50532050, the "973" program under Grant No. 2006CB604906, the CAS Innovation Program, the National Natural Science Foundation of China under Grant No. 60506014.

Reference

[1] M.H. Huang, S. Mao, H. Feick, H. Yan, Y. Wu, H. Kind, E. Weber, R. Russo, P. Yang, Science 292 (2001) 1897.
[2] C.S. Lao, M.C. Park, Q. Kuang, Y. Deng, A.K. Sood, D.L. Polla, Z.L. Wang, J. Am. Chem. Soc. 129 (2007) 12096.
[3] L.E. Greene, M. Law, J. Goldberger, F. Kim, J.C. Johnson, Y. Zhang, R.J. Saykally, P. Yang, Angew. Chem., Int. Ed. 42 (2003) 3031.
[4] A. Tsukazaki, A. Ohtomo, T. Onuma, M. Ohtani, T. Makino, M. Sumiya, K. Ohtani, S.F. Chichibu, S. Fuke, Y. Segawa, H. Ohno, H. Koinuma, M. Kawasaki, Nat. Mater. 4 (2005) 42.
[5] M. Law, L.E. Greene, J.C. Johnson, R. Saykally, P. Yang, Nat. Mater. 4 (2005) 455.
[6] N. Sekine, C.H. Chou, W.L. Kwan, Y. Yang, Org. Electron. 10 (2009) 1473.
[7] S.J. Pearton, D.P. Norton, K. Ip, Y.M. Heo, T. Steiner, Prog. Mater. Sci. 50 (2005) 293.
[8] W.I. Park, J.S. Kim, G.C. Yi, M.H. Bae, H.J. Lee, Appl. Phys. Lett. 85 (2003) 5052.
[9] S.H. Cha, A. Park, K.H. Lee, S. Im, B.H. Lee, M.M. Sung, Org. Electron. 11 (2010) 159.
[10] W.J. Beek, M.M. Wienk, R.A. Janssen, Adv. Funct. Mater. 16 (2006) 1112.
[11] Y.Y. Lin, C.W. Chen, W.C. Yen, W.F. Su, C.H. Ku, J.J. Wu, Appl. Phys. Lett. 92 (2008) 233301.
[12] H.G. Li, G. Wu, M.M. Shi, L.G. Yang, H.Z. Chen, M. Wang, Appl. Phys. Lett. 93 (2008) 153309.
[13] D.M. Baganall, Y.F. Chen, Z. Zhu, T. Yao, M.Y. Shen, T. Goto, Appl. Phys. Lett. 73 (1998) 1038.
[14] S.W. Jung, W.I. Park, H.D. Cheong, G.C. Yi, H.M. Jang, Appl. Phys. Lett. 80 (2002) 1924.
[15] G.C. Yi, W.I. Park, Adv. Mater. 14 (2002) 1841.
[16] D. Zhu, Q. He, H. Cao, J. Cheng, S. Feng, Y. Xu, T. Lin, Appl. Phys. Lett. 93 (2008) 261909.
[17] F. Li, S.W. Cho, D.I. Son, T.W. Kim, S. Lee, Y. Cho, S. Jin, Appl. Phys. Lett. 94 (2009) 111906.